ARCHIVES OF ACOUSTICS
17, 1, 133–150 (1992)

PRINCIPLES OF PHASED-ARRAY IMAGING

J. SOMER

Limburg University, Maastricht, Netherlands

1. Introduction

A phased-array is a transducer which consists of a number of small transducer-elements each of which is individually accessible for excitation and reception (Fig. 1). In contrast to a linear array all elements always simultaneously contribute to the transmission of pulse or the reception of echoes.

Within certain limits, beams can be produced in any wanted direction, according to the Huygens' principle, by applying appropriate time-delays to the electrical signals to or from the elements.

Like for ordinary transducers the overall dimensions l_e (element-length) and l_a array-length in relation to the wave-length determine the beam-properties in terms of both near-field, far-field and beam-width.

Once the width of the elements w being chosen, the number of elements is determined by the array-length l_a. The necessary spaces between the elements should be kept as small as is technically realizable in order to have the maximum effective radiating area. This conflicts however with the requirement of sufficient acoustical isolation between the elements, so that here the first compromise has to be accepted. We will show that this is not the only one we have to cope with.

2. Principles of beam-steering and beam focussing

In order to realize either deviation or focussing of a sound-beam the elements of the array have to be excited by electrical signals which are delayed in a prescribed way with respect to each other, as illustrated in Fig. 2.

In Figure 2a the situation is represented for achieving beam-deviation only. The path-length differences, required to create a flat wave-front propagating in the direction Θ, are linearly dependent on the element-positions and so are the time-delays.

If now instead of a linearly varying time-delay a circular dependence is chosen we can achieve the forming of a circular wave-front rather than a flat one, as illustrated in

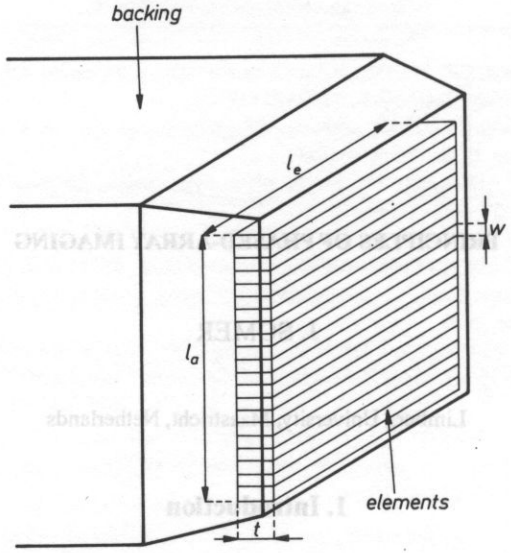

FIG. 1. Construction of a phased-array transducer. l_a = array-length, l_e = element-length, w-element-width, t = thickness (height).

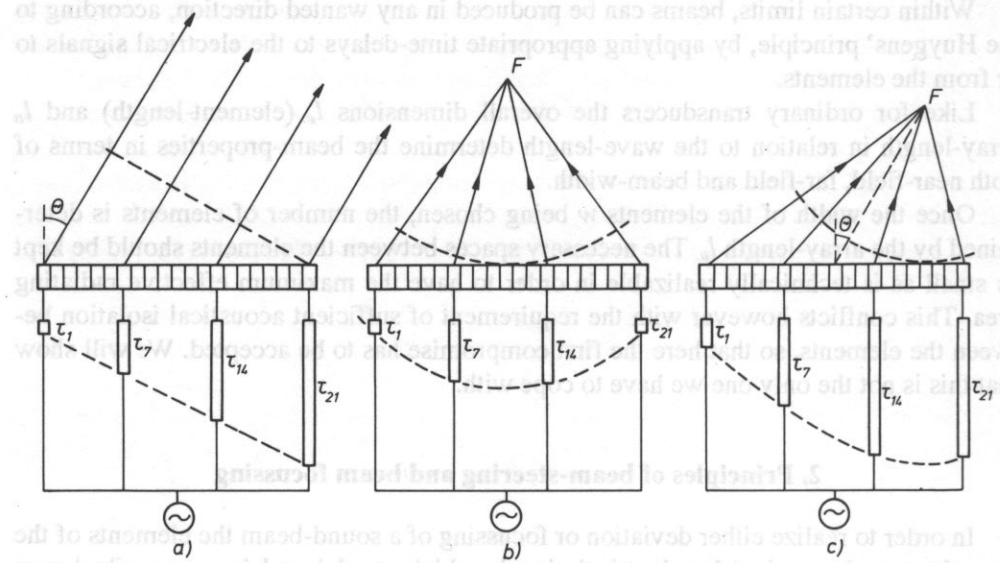

FIG. 2. Schematic presentation of three different transmission modes, together with the pertinent delay-line settings. For simplicity only 4 channels one shown

(a): unfocussed transmission at an off-axis angle Θ. Delay-time varies linearly with element position.

(b): focussed transmission in axial direction. Delay-time varies circularly with element-position.

(c): focussed transmission at angle Θ. Delay-time as function of element-position is a combination of (a) and (b).

Fig. 2b, and a focussed beam is obtained with the center of curvature F as its focal point. Finally, in Fig. 2c we show that the combination of a linear and a circular dependence of time-delay will result in the deviation of a focussed beam.

We mentioned earlier that the number of elements is determined by their widths and the overall array-length l_a (see Figure 1). From Fig. 2 and the pertinent description it is easy to comprehend that the complexity of the system and therefore costs increase proportionally with the number of channels. For this reason we are very keen on keeping the number of elements as low as possible, and the question is how far we can go in enlarging the widths of the elements, before any negative effects become unacceptable.

In order to illustrate the effects of changing any parameter like for instance the element width, we have to solve a tutorial problem. We have to find a useful way to describe sound-fields or beam-patterns in such a manner that significant features are not lost due to too much simplification.

Beam-characterization

In classical transducer theory the acoustic field formation is usually characterized in terms of directional patterns, in general measured or calculated for continuous sound. In Figure 3 a number of such patterns is shown for various source dimensions, calculated in this case for short pulses, rather than for continuous sound. Such a characterization, where the acoustical pressure-amplitude or intensity is plotted against the direction or lateral position, is only meaningful in the far-field because there the curve-shape is independent of range.

In modern echography, however, practically the whole range of interest is within the near-field. Here the field structure is rather complex, although much more for continuous sound than for short pulses involving wide frequency-spectra. This can be easily understood, if we realize that with continuous sound there will be interference between the circular continuous waves with amplitudes all varying between the same positive and negative values. There will be points of total summation and total cancelling; in other words, a rather wild pattern. In the case of pulses, however, it will be appreciated that the shorter the pulse-length, the more incomplete the interference will be, because the spatial extent over which the amplitude differs from zero will become shorter and shorter.

We hope to have explained now sufficiently that dealing with the near-field and at the same time using short pulses, forces us to find other ways of describing the mechanisms and the effects involved; other than just directional patterns.

Computer-generated beam-patterns

We will now set up a realistic model and calculate the field-patterns for different directions Θ different element-sizes, and for both non-focussed and focussed situations.

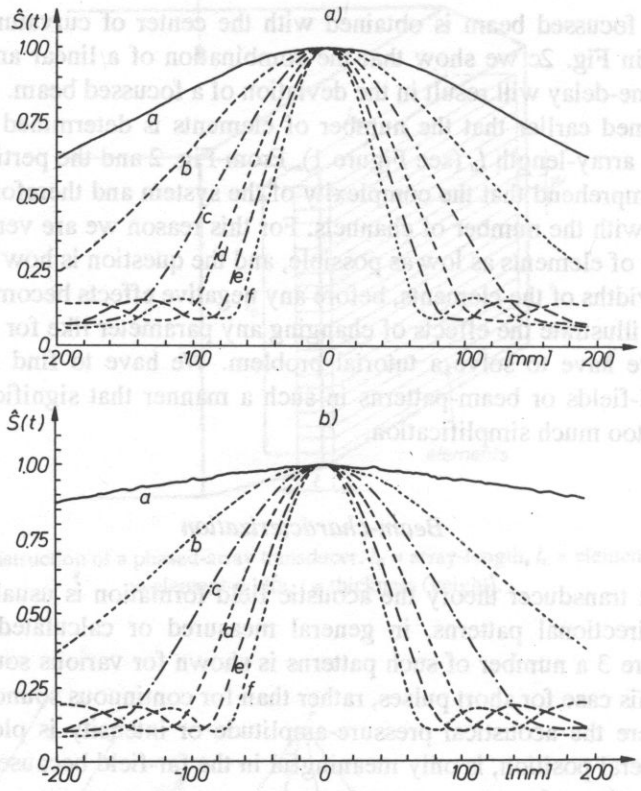

FIG. 3. Directional patterns of sound sources of different dimensions for both Case I in A and for Case II in B. (a): directional pattern of a 0.625 λ wide source (b) through (f): 2, 3, 4, 5 and 6 times source (a).

The array in our model has an overall length $l_a = 20$ mm and radiates pulses with a center-frequency of 3 MHz. Since the wave-length $\lambda = 0.5$ mm the total radiating aperture is 40 wave-lengths wide. The near-field length can be roughly calculated to be 200 mm, covering the whole range of interest.

We will consider the following cases:

Model A: elements of 0.625 $\lambda = 0.3125$ mm
total number of elements is 64
Model B: elements of 1.25 $\lambda = 0.625$ mm
total number of elements is 32.

For simplicity we neglect the isolating spaces between the elements. Since too many parameters affect the beam-patterns we will carry out calculations for two different cases. Case I concerns a line-array. This means that we disregard the second dimension of the elements l_e (see Figure 1) and thus reduce the model to a two-dimensional acoustical problem. Case II refers to an actual array where we have set l_e equal to l_a, that is 40 λ, or 20 mm at $f_c = 3$ MHz. All calculations are based on the same wave-form,

which is a signal with a cosine-squared envelope filled up with five periods of a cosine-function. At 3 MHz the total pulse-length is then 1.67 μsec.

Before we proceed with the field-calculations, we should investigate firstly the directional behaviour of the elements.

Figure 3A shows directional patterns in Case I for element-widths from $0.625 \times \lambda = 0.3125$ mm in curve (a), up to $6 \times 0.625 \times \lambda = 1.875$ mm in curve (f). We observe that the directional selectivity of a sound-source gradually increases with its width.

It is permitted to use directional patterns in these cases, since even for the largest width the near-field length is only 1.76 mm. We see then that curve (a) applies to what we adopted as Model A, and find that the radiated sound-pressure at the boundary-angles + 45° and – 45° has dropped from 1 to 0.72, which corresponds to 2.85 dB. We feel, more or less intuitively, that this could be acceptable for a practical system. In other words, it seems a good enough approximation of a point-source.

For Model B we assumed an element-width twice as large and this corresponds to curve (b) in Figure 3A. Here a drop from 1 to 0.55 can be noticed at the outer angles, which is 5.19 dB. This seems quite unacceptable, because, again intuitively, the summation of the contributions of all elements for these maximum angles will also be at least 5.2 dB lower than for $\Theta = 0°$. And if the elements radiate some spurious power in or near zero-direction, this will be strongly enhanced by the so much greater on-axis sensitivity. Let us see if our intuition is right.

For both models and for both cases field-patterns are calculated, using the pulse-shape as we described already. In a 3D-picture only three quantities can be mutually related. In this case these are the lateral displacement, the scanning-depth and the sound-pressure or the sound-intensity. We have to decide about the pulsatile signals we are dealing with. These are functions of time at each point in the plane considered and we have no means for taking up time as a fourth dimension. We recall, however, that in practical systems the signal-envelope, rather than the RF-signal, is displayed on the screen, and that the echo-brightness is determined mainly by the peak-value of it. We decided therefore to use also in our computer-model peak-detection of the signals. In the field-patterns as will be shown the variable characterizing the field-strength is thus the peak-value of the calculated sound-pulse in the field.

This variable, which we will call the peak-sound-pressure, is presented in the field patterns as the height of the curves above the "ground"- or zero-plane. It cannot be emphasized strongly enough that the exposed patterns do not represent the **beam-shape**, but the **sound-amplitude**. What the **brightness** is the Schlieren-pictures, is the **vertical deflection** or **"height"** in the shown field-patterns.

Case I

We now come to the discussion of the computer-generated field-patterns for both the Model A in Fig. 4 and the Model B in Fig. 5 in Case I. The left column shows the

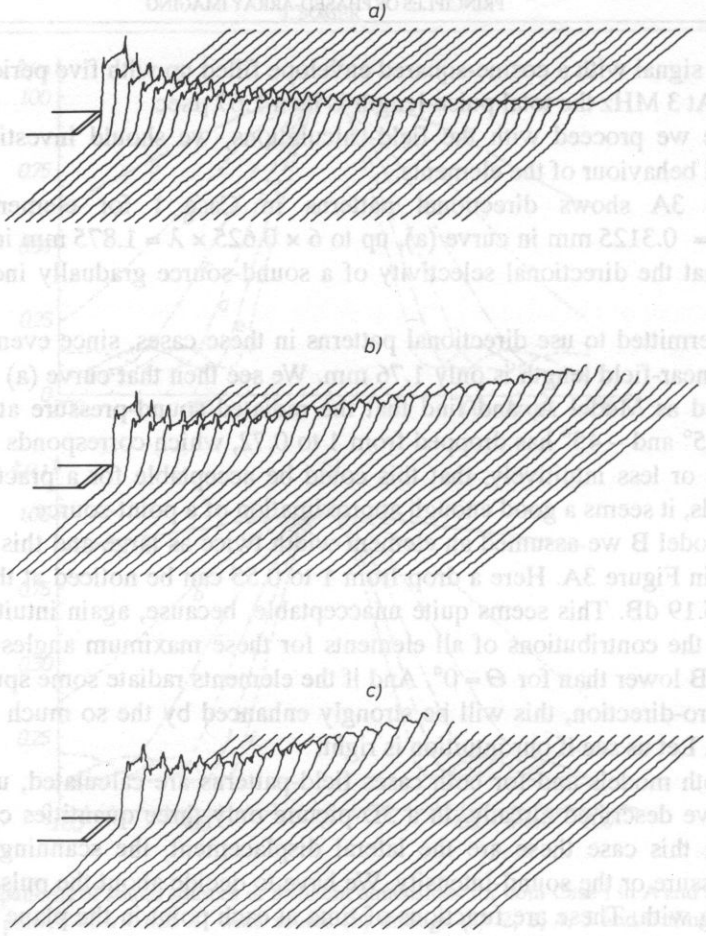
a)
b)
c)

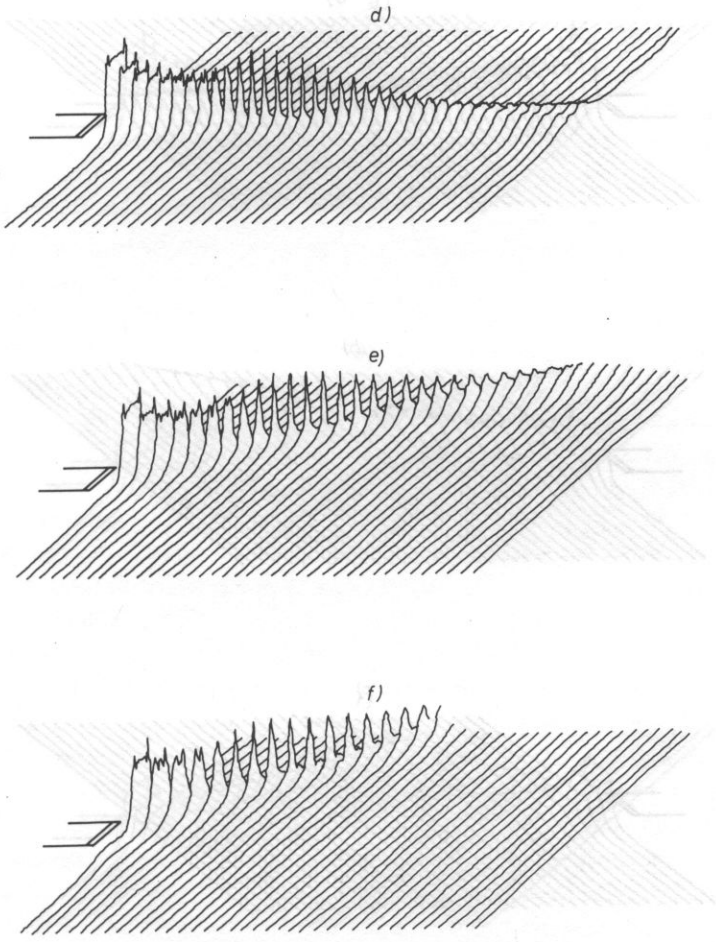

FIG. 4. Beam-patterns as calculated for a 40 λ wide line-array with 64 elements, each 0.625 λ wide
(a), (b) and (c): unfocussed beams at 0°, 30° and 45° respectively
(d), (e) and (f): beams focussed at 160 λ for the same angles.

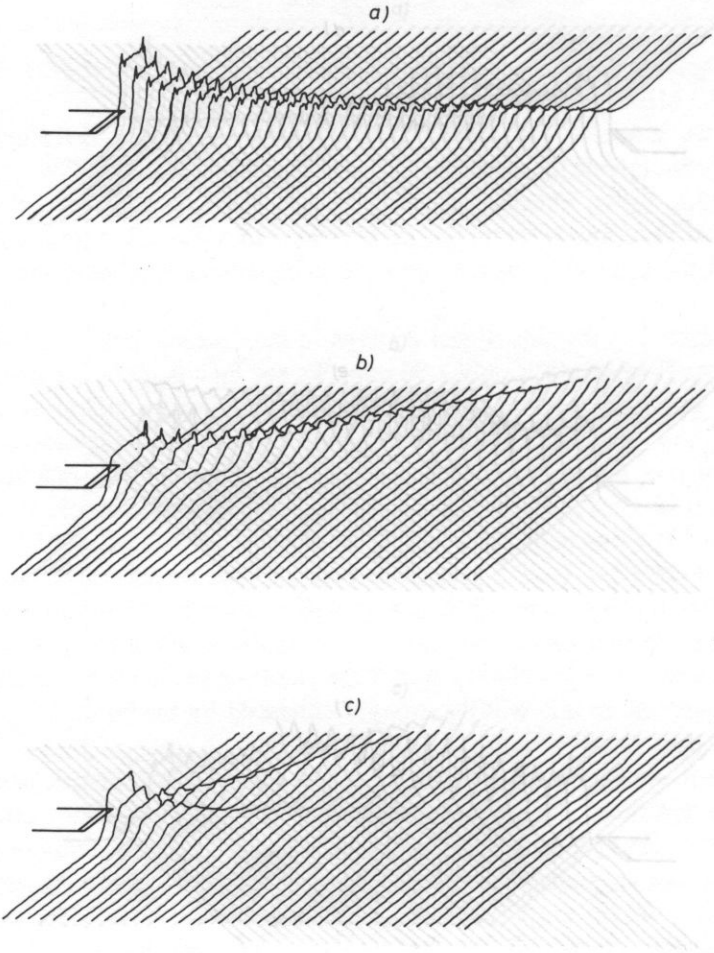
a)
b)
c)

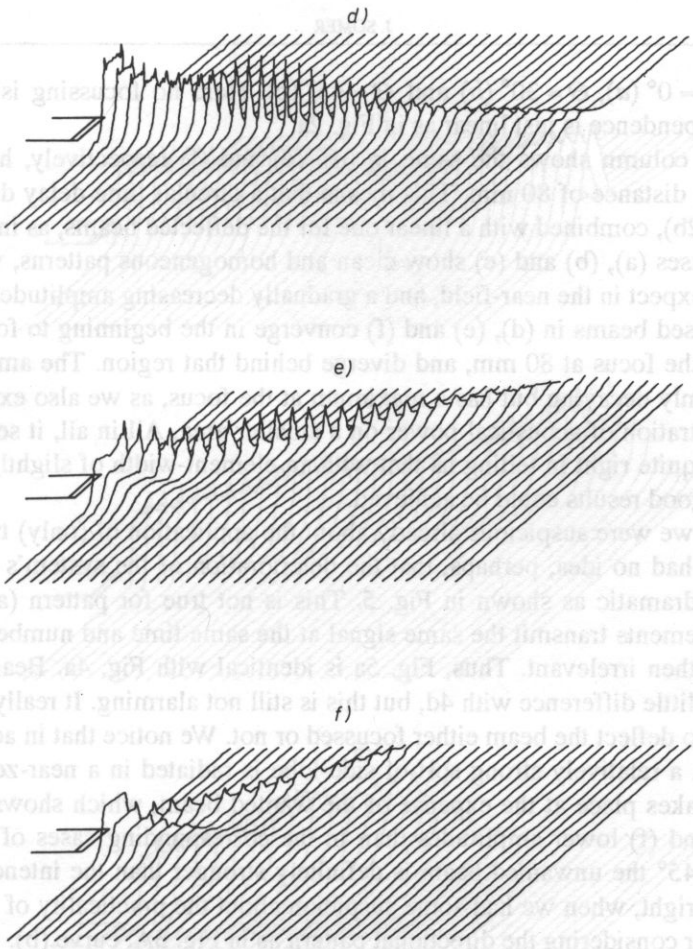

FIG. 5. Beam-patterns as calculated for a 40 λ wide line-array with 32 elements, each 1.25 λ wide. Specifications of (a) through similar to Fig. 4.

results for $\Theta = 0°$ (*a*), $\Theta = 30°$ (*b*) and $\Theta = 45°$ (*c*). Here no focussing is applied; the time-delay dependence is just linear as in Fig. 2a.

The right column shows the same in (d), (e) and (f) respectively, however with focussing at a distance of 80 mm. This means that a circular time-delay dependence is applied (Fig. 2b), combined with a linear one for the deflected beams, as in Fig. 2c. The unfocussed cases (a), (b) and (c) show clean and homogeneous patterns, with uniform width, as we expect in the near-field, and a gradually decreasing amplitude.

The focussed beams in (d), (e) and (f) converge in the beginning to form a narrow region about the focus at 80 mm, and diverge behind that region. The amplitude is no longer uniformly decaying but has a maximum at the focus, as we also expect because of the concentration of acoustical power on a smaller area. All in all, it seems that our intuition was quite right in telling us that with an element-width of slightly over half a wave-length good results could be achieved.

Although we were suspicious already about the application of (only) twice as wide elements, we had no idea, perhaps, that the deterioration of the system's performance would be so dramatic as shown in Fig. 5. This is not true for pattern (a), of course, because all elements transmit the same signal at the same time and number and size of elements are then irrelevant. Thus, Fig. 5a is identical with Fig. 4a. Beam-pattern 5d shows a very little difference with 4d, but this is still not alarming. It really goes wrong when we try to deflect the beam either focussed or not. We notice that in addition to the wanted beam, a relatively strong sort of side-lobe is radiated in a near-zero direction. This clearly takes place at the expense of the wanted beam, which shows in all cases (b), (c), (e) and (f) lower amplitudes than in the corresponding cases of Fig. 4. At a deflection of 45° the unwanted beam is definitely stronger than the intended one. Our intuition was right, when we had some suspicion about the practicality of double-sized elements, after considering the directional pattern as in Fig. 3A, curve (b).

In discussions about array-transducers often the term "aliasing" is used. This is a common expression in signal-theory and is used to characterize the effects of under-sampling of a signal. If we make the element-spacing too large, the sampling of the spatial signal is then too coarse. This applies only when there are frequency-components in the lateral direction, which means for deflected beams only. The reader may feel somewhat confused, since "sampling spatial signals" suggests that we are referring to reception of signals rather than to transmission. Then it may now be the right moment to emphasize that transmission and reception are fully reciprocal. The calculated patterns for transmission can as well be considered to represent reception sensitivity.

Case II

Showing the results of a line-array first has the advantage that any near-field effects due to the element-length l_e are eliminated and cannot obscure the particular effects of the lateral configuration. We can state now, roughly, that the differences between Fig. 6 and 7, representing Case II, and Fig. 4 and 5, referring to Case I, are due to the ele-

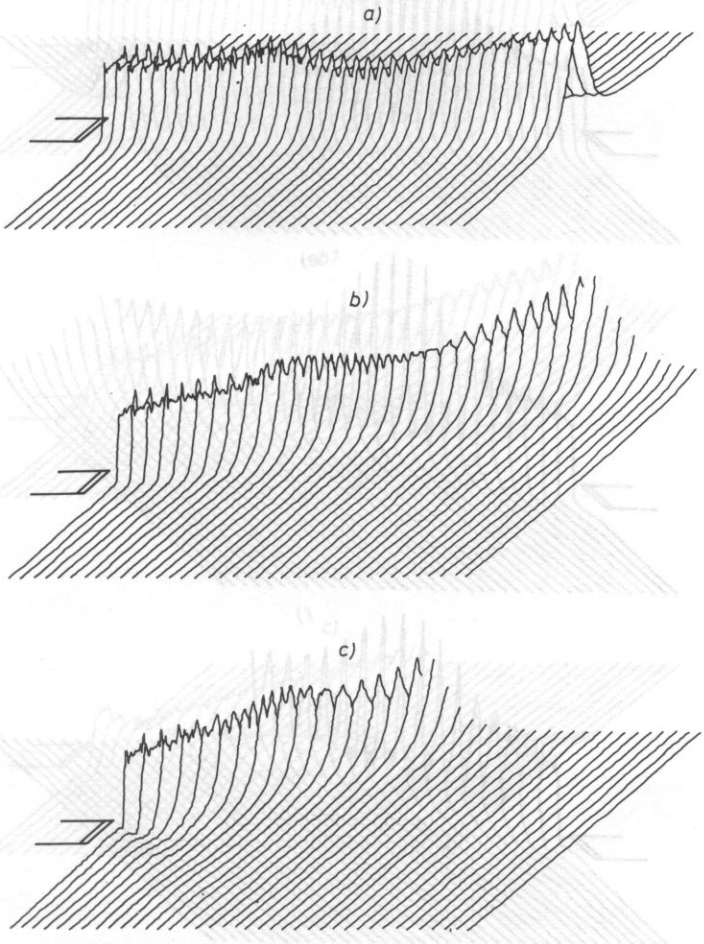
a)
b)
c)

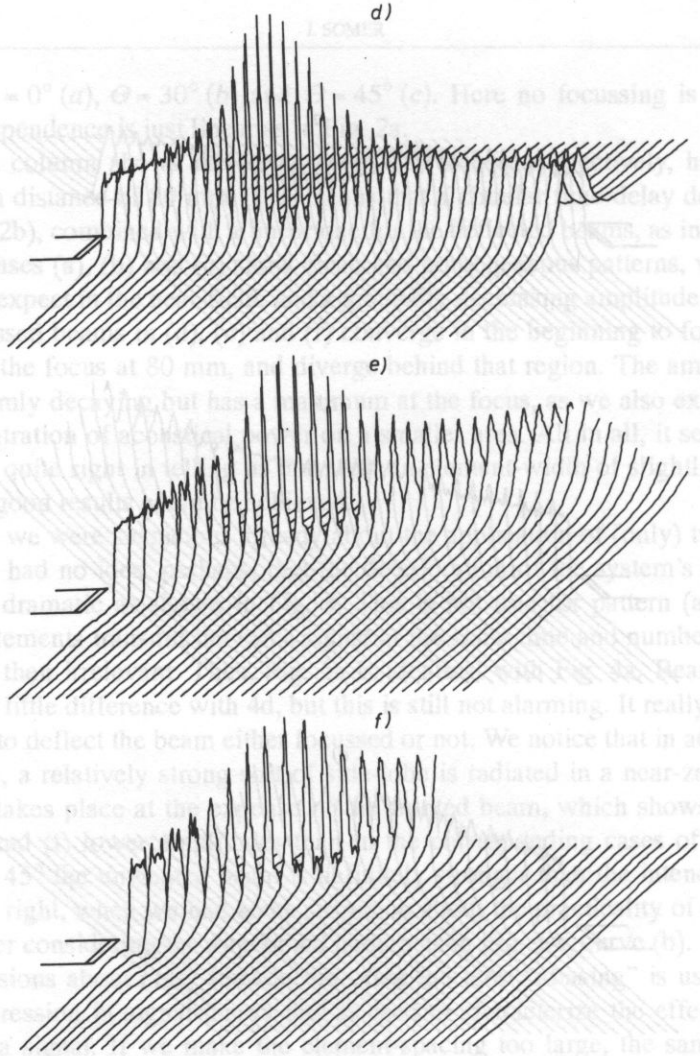

FIG. 6. Beam-patterns as calculated for a 40 λ wide rectangular-array with 64 elements, each 0.625 λ wide and 40 λ long
Specifications of (a) through (f) similar to Fig. 4.

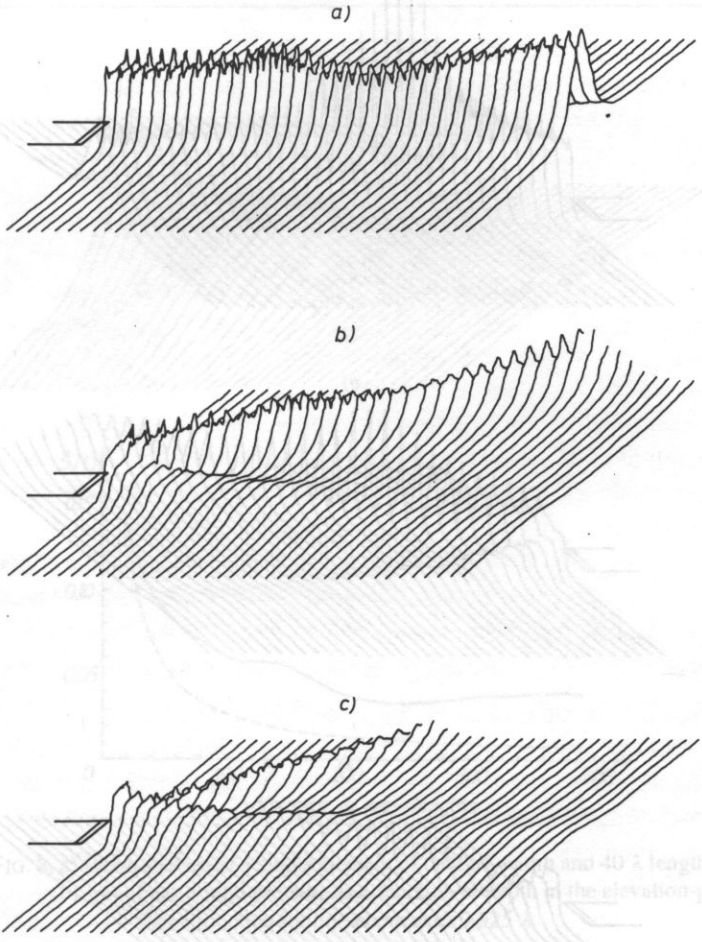
a)
b)
c)

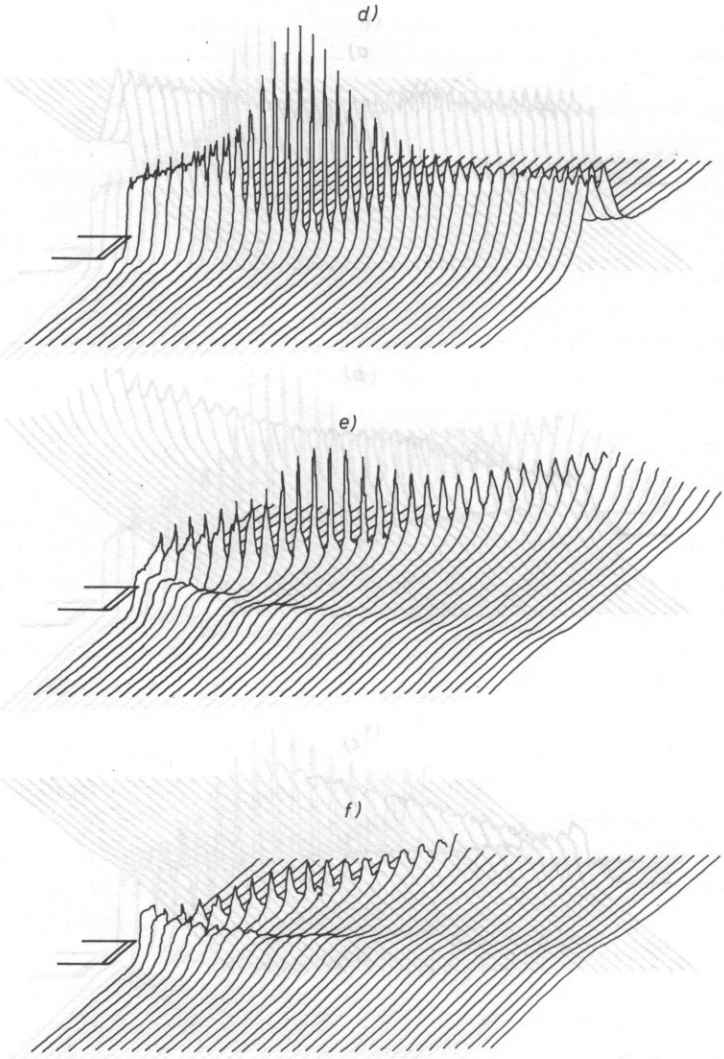

FIG. 7. Beam-patterns as calculated for a 40 λ wide rectangular-array with 32 elements, each 1.25 λ wide and 40 λ long.
Specifications of (a) through (f) similar to Fig. 4.

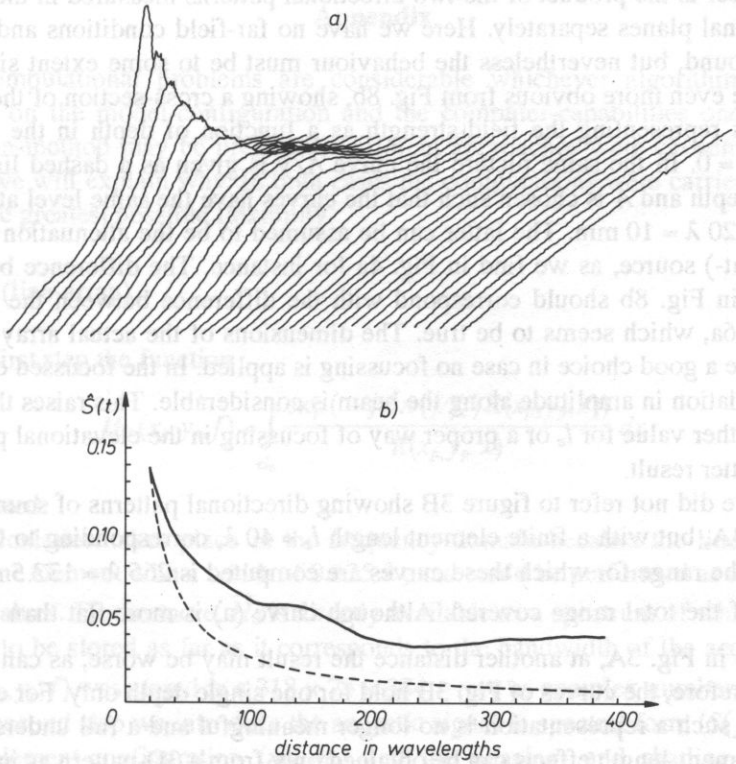

FIG. 8. a) Beam-pattern of a single element of 0.625 λ width and 40 λ length
b) —— Peak-sound pressure as a function of depth in the elevation-plane at $\Theta = 0$
------ Same function for line-element of 0.625 λ.

ment-length l_e. It may therefore be appreciated that changing l_e will yield different results, as will any (fixed) focussing applied in the elevation-plane.

Comparing Figures 5 and 7 shows that also for an actual array element-widths considerably greater than $\frac{1}{2}\lambda$ are out of the question because of the aliasing effects. We can thus restrict ourselves to comparing Figs. 4 and 6, which is quite revealing.

In Figure 6a, b and c we observe a more or less uniform level, whereas in the corresponding patterns of Figs. 4a, b and c a monotonous decrease with depth can be noticed. This means that there is an enhancement,effect obviously due to the directional-pattern in the elevation-plane.

This enhancement-effect is even more striking in the focussed-beams of Fig. 6d, e and f, as compared to the corresponding ones of Fig. 4.

In order to illustrate this further the beam-pattern was computed for just one element of 0.625 λ width and 40 λ length. The result is shown in Fig. 8a and reveals nicely the enhancement-effect over almost the whole range of interest. In the far-field and for continuous sine-waves there is a rule that the total 3-dimensional directional pattern

of a transducer is the product of the two directional patterns measured in the azimuthal and elevational planes separately. Here we have no far-field conditions and no mono-frequency sound, but nevertheless the behaviour must be to some extent similar. This may become even more obvious from Fig. 8b, showing a cross-section of the pattern in 8a, and thus representing the field-strength as a function of depth in the elevational plane for $\Theta = 0$. In the same picture the curve A/y is given as a dashed line where y represents depth and A is chosen such that the curves have the same level at the begin-point at $y = 20\ \lambda = 10$ mm. The latter can be assumed to be the attenuation curve of a line-(or point-) source, as we find in Fig. 4a for instance. The difference between the two curves in Fig. 8b should correspond with the difference between the patterns in Fig. 4a and 6a, which seems to be true. The dimensions of the actual array of Case II turn out to be a good choice in case no focussing is applied. In the focussed cases, however, the variation in amplitude along the beam is considerable. This raises the question whether another value for l_e or a proper way of focussing in the elevational plane could yield any better result.

So far we did not refer to figure 3B showing directional patterns of sources similar to those of 3A, but with a finite element length $l_e = 40\ \lambda$, corresponding to Case II. As in Fig. 3A, the range for which these curves are computed is $265\ \lambda = 132.5$ mm, which is about $\frac{2}{3}$ of the total range covered. Although curve (a) is more flat than the corresponding one in Fig. 3A, at another distance the result may be worse, as can be seen in Fig. 8a. Therefore, the curves of Fig. 3B hold for one single depth only. For elements of finite length such a representation is no longer meaningful and a full understanding of the finite element-length effects can be obtained only from a 3D-pattern as in Fig. 8a.

In the Appendix a brief account is given of the computational aspects, by which the results presented above, are achieved.

3. Conclusions

Since modern phased-array systems operate entirely in the near-field a new approach is necessary to describe their performance.

Investigation of computer-models has shown that increasing the element-width leads progressively to deterioration of the produced beams. The element width should not exceed $\frac{1}{2}\ \lambda$ too far. With $0.625\ \lambda$ a reasonable performance seems to be possible.

The element-length has a great influence on the overall beam intensity. It is likely that it can be used in the desing for shaping the beam in the azimuth-plane. Also focussing in the elevational plane may affect the overall beam-shape in the azimuth-plane. Of course, the beam contours in the elevation-plane are important too. It requires further research to acquire more knowledge about this aspect. Also the influence of the applied wave-form is not yet fully understood. All in all, as compared to far-field problems and mono-frequency sound, the complexity of the near-field problem and pulsatile signals is considerable.

Appendix

The computational problems are considerable whichever algorithm is chosen. Depending on the model-configuration and the computer-capabilities one or another computation-method may be preferred. Different approaches were chosen for the two cases and we will explain why. In both cases the computations were carried out in two steps for the greatest possible flexibility.

Case I (line-array)

In the first step the function

$$\overline{H}_0(x_p, y_p, f) = \int_{el_0} \frac{\exp(-j2\pi(f/f_c)R(x_p, y_p, x))}{R(x_p, y_p, x)}\, dx \tag{1}$$

was calculated.

The calculation takes place in the frequency-domain because the line integration was over one element with a width of 0.625 λ, and could be performed as a summation of only 5 values. Furthermore, $\overline{H}_0$ is directly available as a spectrum of which only that part needs to be stored as far as it corresponds to the bandwidth of the acoustic signal $\overline{S}(f)$. $\overline{H}_0(x_p, y_p, f)$ was stored in a 318 × 75 × 384 – rray as complex numbers.

In the second step we introduce the acoustic signal in spectral form ($S(f)$), together with the element-configuration (m_1, m_2) and the phasing- and shading-information ($\overline{w}_i(f)$).

Then

$$s_t(x_p, y_p) = \max\left|F^{-1}\left[\overline{S}(f) \sum_{i=m_1}^{m_2} \overline{w}_i(f) \cdot \overline{H}_0(x_p - i\Delta e, y_p, f)\right]\right| \tag{2}$$

Case II (rectangular array)

A similar approach as in Case I would now involve a surface-integral of a complexity depending on the element length l_e. Such a surface-integral can be avoided by applying the so-called impulse-response method [1]. The whole computation is then carried out in the time-domain. Instead of performing a surface-integral, the impulse-response $h_0(t)$ can directly be derived as a function of time. Considering the possibility of fast-fourier transforming this function leads to the conclusion that the bandwidth of $h_0(t)$ is too large. The huge number of points needed for the FFT, in order to avoid aliasing effects, would lead to much too high CPU-times. Fourier-transforming the $h_0(t)$ function analytically seems quite a formidable task.

Choosing the time-domain approach, however, requires the performing of a convolution-integral, which needs a lot of care to insure that a sufficient accuracy is obtained.

The first step to be carried out is now

$$p_0(x_p, y_p, t) = h_0(x_p, y_p, t) \otimes s(t) \quad \text{with } h_0(x_p, y_p, t) = \Theta_2(x_p, y_p, t) - \Theta_1(x_p, y_p, t), \tag{3}$$

where the Θ's are given as arcsine- and arccosine-functions.

Again, the field information for only one central element is calculated. Some flexibility, however, is lost since we have to introduce the wave-form in the first step already. The required storage is now half as much because of real numbers, rather than complex ones.

The second step requires the remaining information about element-configuration (m_1, m_2), phasing (t_{di}) and shading (w_i).

$$\hat{s}_t(x_p, y_p) = \max \left| \sum_{i=m_1}^{m_2} w_i p_0(x_p - i\Delta e, y_p, t + t_{di}) \right| \tag{4}$$

References

[1] P. R. STEPANISHEN, *Transient radiation from pistons in an infinite planar baffle*, Journ. Ac. Soc. America, **49**, 1629–1638 (1971).

Received on September 26, 1990